Thickness and Temperature Dependence of ZnO/Glass Thin Film Systems Obtained by Thermal Evaporation

Ş. Kinal and G. Utlu*

Ege University, Faculty of Science, Department of Physics, 35100 Bornova, Izmir, Turkey

(Received March 8, 2019; revised version June 10, 2019; in final form July 23, 2019)

In this study, the effects of annealing temperature and thickness on zinc oxide formation in ZnO/glass thin film systems were investigated. For this purpose, ZnO thin films with thicknesses of 150–300 nm were obtained by thermal evaporation and then annealed in a range of 200–400 °C in air. The structural, optical, and electrical characterizations of ZnO/glass films were obtained. According to structural investigations, the deposited films contain Zn rich phases due to low oxygen content. By increasing the annealing temperature, the X-ray diffraction intensity of the Zn peaks that belongs to Zn rich phases is decreased and the ZnO phases were starting to form by oxidation at 300 °C. After 300 °C, polycrystalline ZnO phases are formed in all samples and at 400 °C, ZnO films become completely transparent. Scanning electron microscopy and atomic force microscopy analysis show that nanorods are formed on the surface of the ZnO films. It appears that these nanorods exhibit a random distribution and after annealing, columnar ZnO nanostructure growths occur more regularly. The electrical sheet resistances and resistivity analyses indicate that there is a transition from conductive Zn rich phases to semiconductor ZnO phases. This dramatic resistance increase is due to the transition from dark brown Zn rich phases to transparent ZnO phases. Moreover, the optical transmittance increases to up to 85% after annealing. Optical band gap values are calculated as 3.11–3.41 eV from UV-vis transmistance analysis.

DOI: 10.12693/APhysPolA.136.432

PACS/topics: ZnO thin film, thermal evaporation, annealing, ZnO nanorod, XRD, SEM, AFM techniques

1. Introduction

Metal oxides and especially ZnO material have an important place in electronic and optoelectronic device applications [1–3]. Adjusting the electrical, optical, and structural properties of ZnO material makes this material very advantageous for the desired applications and makes it important for material science. ZnO at room temperature has 3.37 eV band gap and 60 meV exciton binding energy [4–10]. Because of its superior electrical/optical properties, ZnO can be used in many applications such as LEDs, laser diodes, gas sensors, and photodetectors [11–16].

Many methods are used to produce ZnO thin films such as sputtering, spray pyrolysis, sol–gel, and thermal evaporation [17–24]. In this study, ZnO thin films were obtained by thermal evaporation method on glass substrates. This technique is advantageous over other methods since it has a low cost, simple, and easily controllable parameter [18]. In most of these methods Zn thin films are first deposited and annealed in air environment to form ZnO thin film [17, 18]. However, in this study, ZnO films were deposited on glass substrates by evaporation of ZnO particles and then ZnO films were obtained by annealing in air environment. In addition, different thicknesses of ZnO/glass film systems were obtained and annealed at different temperatures. According to the literature, ZnO particles are decomposing to Zn and O atoms during evaporation.

The presence of atomic oxygen in the deposition chamber is effective during film formation and thus Zn-rich phases occur [21]. As-deposited ZnO films with low oxygen content cause complete oxidation at low annealing temperature relative to films obtained from Zn. For this reason, in this study, it is aimed to obtain Zn rich films with low oxygen content during evaporation of ZnO particles and then to produce ZnO films by annealing. Furthermore, in thin film systems the morphology of the films strongly depends on thickness and temperature [4–22]. Therefore, the structural, electrical, and optical properties of the ZnO/glass thin film systems obtained in this study were investigated in depth. The obtained results were compared with the film growth conditions and parameters to produce ZnO thin films with optimum properties for different applications.

2. Experimental details

In this study, ZnO thin films were deposited firstly on the glass substrate of ZnO pellets with 99.99% purity and 1–3 mm diameters by thermal evaporation using the Edward high vacuum system with a base pressure of about 1×10^{-6} Torr. The glass substrates were cut into small pieces of 10 mm×10 mm for resistivity measurements. The substrates were then cleaned using standard chemical cleaning. Prior to film deposition, ZnO particles were subjected to a glow discharge under high vacuum so that

*corresponding author; e-mail: gokhan.utlu@ege.edu.tr

the film was well attached to the substrate. ZnO films with a thickness of 150–300 nm were deposited on this substrate by thermal evaporation. The thickness of the obtained ZnO thin film systems (with low oxygen content) was determined by the quartz crystal oscillator during film deposition with a sensitivity of ±0.1 nm.

Secondly, ZnO thin film systems were annealed for 2 h at temperatures: 200 °C, 300 °C and 400 °C. The thickness values of the films are 150 nm, 250 nm and 300 nm. Structural analyses of all these films were made by using X-ray diffraction, scanning electron microscopy, and atomic force microscopy. Philips X'Pert Pro X-ray diffractometer with Cu K_α line was used to determine for structural crystallographic phases. The SEM measurements were performed using the Philips XL-30S FEG Scanning Electron Microscope and the AFM measurements were taken with Ambient AFM Nanomagnetics Instruments.

In addition to structural analysis, electrical and optical analyses of all these films have been made. The sheet resistances of ZnO films were measured at room temperature using the classic van der Pauw technique. Optical transmittance measurements were performed with spectrophotometer in the wavelength range of 200–900 nm. Optical band gap values were obtained from the absorption spectra using the relation [21]:

$$\alpha h\vartheta = A\left(h\vartheta - E_g\right)^{1/2}. \tag{1}$$

3. Results and discussion

3.1. XRD measurements

XRD spectra of the ZnO thin film systems annealed at different temperatures (200 °C to 400 °C) are shown in Figs. 1–3 as a function of the selected films of 150, 250, 300 nm thickness. As seen from Figs. 1–3 as-deposited samples show only Zn peaks observed at $2\Theta \approx 37°$, $2\Theta \approx 39°$ and $2\Theta \approx 43°$ which are Zn (002), Zn (100), Zn (101), respectively. This result shows that as-deposited samples have low oxygen content and Zn rich phases occur. On the other hand, annealed samples show oxidation behavior by increase of the temperature. Oxidation mechanism is quite important during ZnO formation and depends on the composition and structure of the film. When we increase the annealing temperature from 200 °C to 400 °C, the Zn phases decrease in intensity first, and then the ZnO phases begin to form. After annealing at 200 °C, some Zn phases reduction is occur. At 300 °C, Zn phases disappear and ZnO phases become visible because of the oxidation. This indicates that the Zn phases are replaced by ZnO. At 400 °C, ZnO phase intensities increase and sharp ZnO phases are formed. These results and oxidation mechanism of ZnO are quite similar to Bouhssira et al. They have observed that the lowest temperature of complete oxidation is 300 °C for ZnO formation [21]. Furthermore, XRD analyzes of our film set of 250 nm and 300 nm obtained in this study showed similar behaviors to the 150 nm film set given above. Although, as the film thickness increases from 150 nm to 300 nm, intensities of the ZnO phases decrease. The ZnO structure exhibit non preferential orientation, because many ZnO peaks such as (100), (101), (002), (102), (110) are present. Besides, unlabeled peaks correspond to some impurity phases in Figs. 1–3. Depending on the growth mechanisms in ZnO formation, different directions may occur in every method. For example most of thin films have Zn (002) preferential orientation which is observed for sputtering, pulse laser deposition, or spray pyrolysis. We have used thermal evaporation method and obtained ZnO thin films which have polycrystalline hexagonal wurtzite structure in this study.

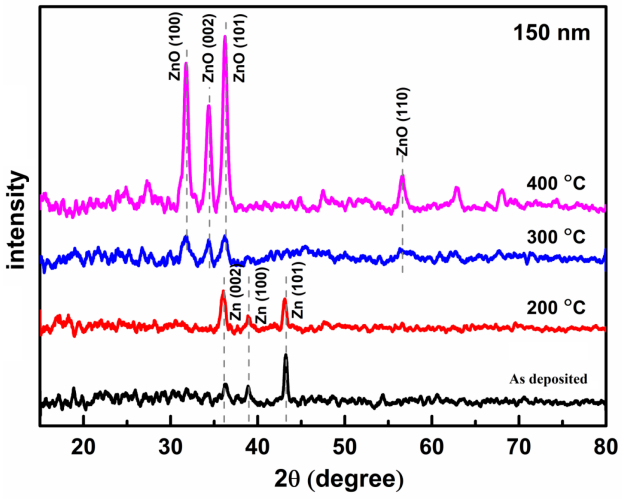

Fig. 1. XRD spectra of the ZnO thin films of 150 nm thicknesses with different annealing temperatures: (a) as-deposited, (b) at 200 °C, (c) at 300 °C, (d) at 400 °C.

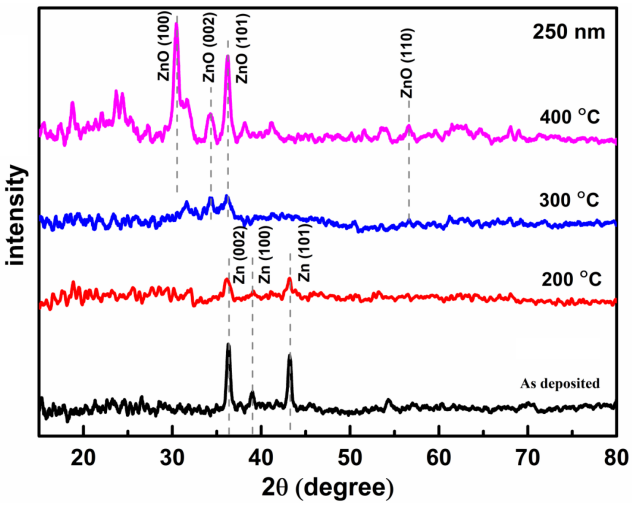

Fig. 2. As in Fig. 1, but for films of 250 nm thicknesses.

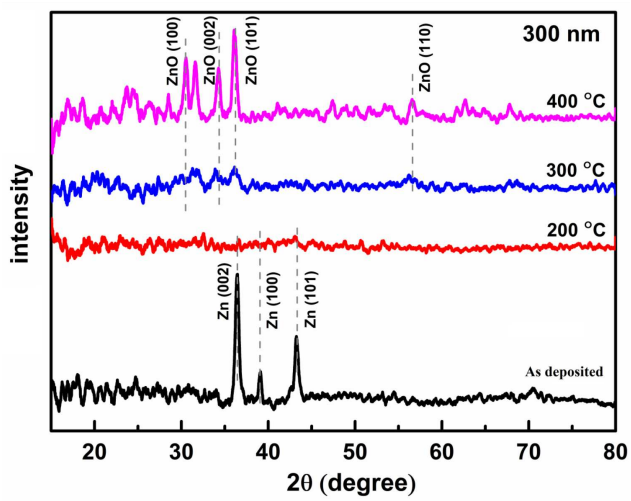

Fig. 3. As in Fig. 1, but for films of 300 nm thicknesses.

3.2. SEM and AFM measurements

The SEM images obtained from ZnO films annealed at different temperatures (200 °C to 400 °C) are shown in Figs. 4–6 for the films of 150, 250, 300 nm thickness. SEM studies reveal that nanorods are formed on the surface of all ZnO films. It has been observed that these nanorods on the surface have a random distribution after annealing. As the annealing temperature increases from 200 °C to 400 °C, these nanorods grow in a columnar way and completely cover the surface. In addition, clusters have formed on the surfaces of these columnar nanorods. These regions appear white in SEM images. Considering the XRD studies, it is thought that these structures, which show transition from zinc (Zn) rich phases to zinc-oxide (ZnO) phases, are due to the increased oxygen content. Our SEM measurements also show that as the same behavior is observed in our other 250 nm and 300 nm glass-carrier ZnO film sets.

AFM images of the ZnO films shown in Figs. 7–8 clearly reveal that the nanorods grow in a columnar way and come together to bring the nanorod clusters along the surface. AFM analysis shows that nanorod cluster sizes firstly decrease to 200–300 nm with temperature increasing to 300 °C, then increase to 700–1000 nm for 400 °C. For this reason boundary density due to the agglomeration of nanorods is firstly increasing and then decreasing. After annealing, Zn phases are replaced by ZnO phases and at 300 °C, which is transition temperature in this study, Zn completely transform to ZnO phases. Minimum ZnO nanorod cluster sizes have been obtained at 300 °C in all our ZnO film sets. At 400 °C, ZnO phases with higher intensity occur. These changes in the structure are also manifested by the average roughness values in AFM analyzer. The mean roughness values corresponding to the nanorod agglomeration (cluster), shown in Fig. 8 and Table I, display us the same behaviour due to the phase transformation from Zn rich phases to ZnO.

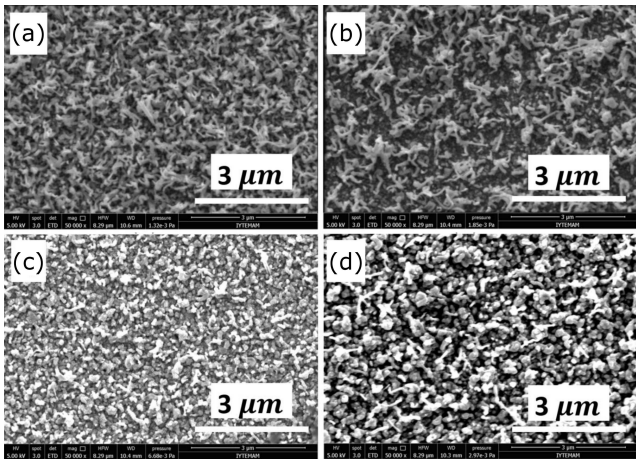

Fig. 4. The SEM images obtained from ZnO films annealed at different temperatures (200 °C to 400 °C) for the films of 150 nm thicknesses. (a) As-deposited, (b) at 200 °C, (c) at 300 °C, (d) at 400 °C.

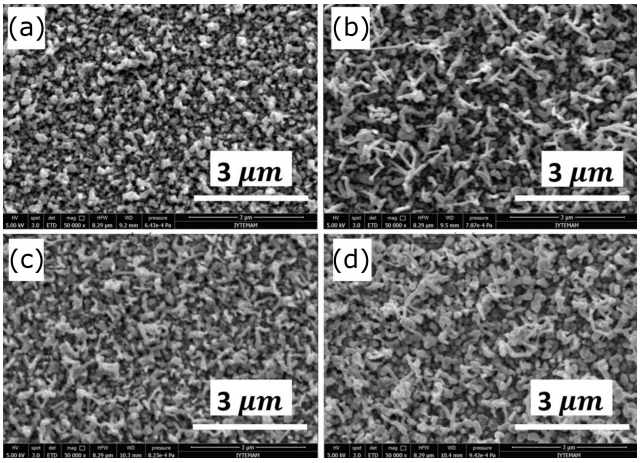

Fig. 5. As in Fig. 4, but for films of 250 nm.

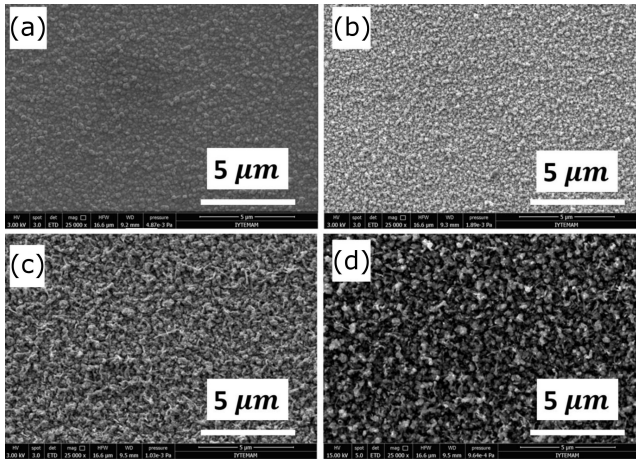

Fig. 6. As in Fig. 4, but for films of 300 nm.

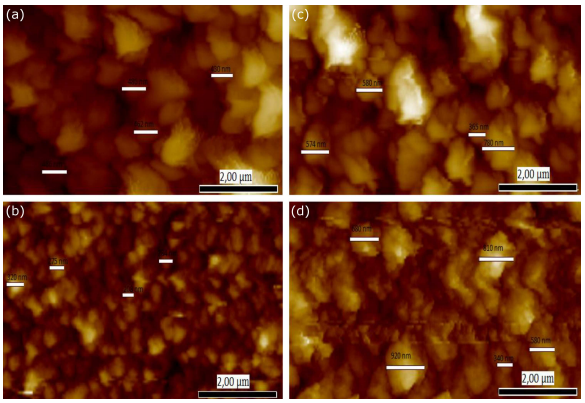

Fig. 7. AFM images of the selected ZnO film of 150 nm thickness with different annealing temperatures: (a) As-deposited, (b) at 200 °C, (c) at 300 °C, (d) at 400 °C.

The mean roughness values of the as deposited Zn rich films are quite high because of the higher deposition rate (4–5 nm/s) of our thermal evaporation. According to the literature, if the film is deposited with higher rates, it has higher surface roughness and higher grain size [25, 26]. After annealing of these films to 300 °C, mean roughness values are decreased 2–3 times and phases transform to ZnO structure because of the oxidation.

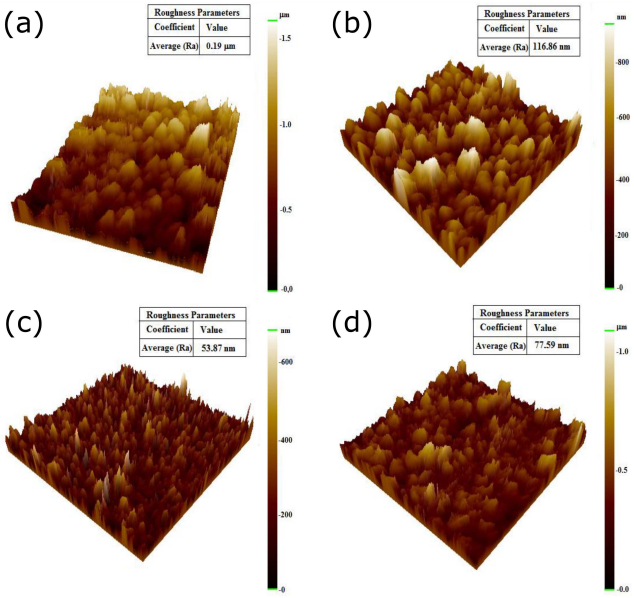

Fig. 8. 3D AFM images and mean roughness values of the selected ZnO films of 150 nm thickness with different annealing temperatures (a) As deposited, (b) at 200 °C (c) at 300 °C, (d) at 400 °C.

TABLE I

Mean cluster size and roughness values of the ZnO films which is obtained from AFM analysis

ZnO/glass samples	As-deposited		Annealed at 200 °C		Annealed at 300 °C		Annealed at 400 °C	
	Cluster size [nm]	Roughness value [nm]	Cluster size [nm]	Roughness value [nm]	Cluster size [nm]	Roughness value [nm]	Cluster size [nm]	Roughness value [nm]
SET 1 thickness 150 nm	465	190	585	116.9	272	53.9	666	77.6
SET 2 thickness 250 nm	652	230	658	82	282	89	1030	160
SET 3 thickness 300 nm	765	78.7	643	108.6	413	46.1	674	100

3.3. Optical properties

The optical transmittance spectra of the ZnO film with thickness of 150 nm are presented in Fig. 9. Optical transmission increases with temperature from 200 °C to 400 °C. The transmittance value for the deposited film with thickness 150 nm is between 0.1–0.5% in visible range. As-deposited samples appear dark brown as the light transmission is very low. This is due to the fact that we obtain Zn-rich phases before annealing.

After annealing, oxidation occurs and ZnO phases begin to form. If the annealing temperature increases to 400 °C, the value of the transmittance is increased to 85% in our films. The Zn phases are replaced by ZnO phases after annealing, and the films show a transparent appearance which is shown in Fig. 10 clearly. If the annealing temperature increases, defect number of the film is decreased because of the improvement of the stoichiometry. When the light loss due to the scattering of defects is decreased, the light transmittance is increased. Figure 9 shows that in our 150 nm ZnO thick films annealed at 300 °C has the light transmittance between 60% and 85%

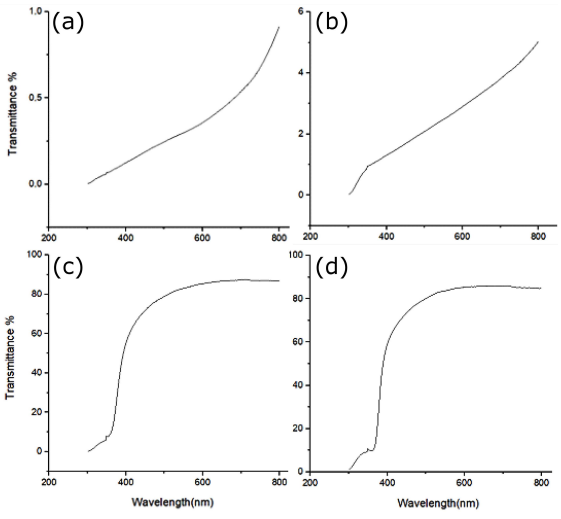

Fig. 9. The optical transmittance spectra of the ZnO film with thickness of 150 nm with different annealing temperatures: (a) as-deposited, (b) at 200 °C, (c) at 300 °C, (d) at 400 °C.

in visible area. As the film thickness increases from 150 nm to 300 nm, light transmittance decreases between 30% to 75% in visible range for annealed samples at 300 °C. In all our film sets (150–300 nm), the most prominent examples in which the transition to the zinc-oxide (ZnO) phases are observed are those annealed at 300 °C for 2 h.

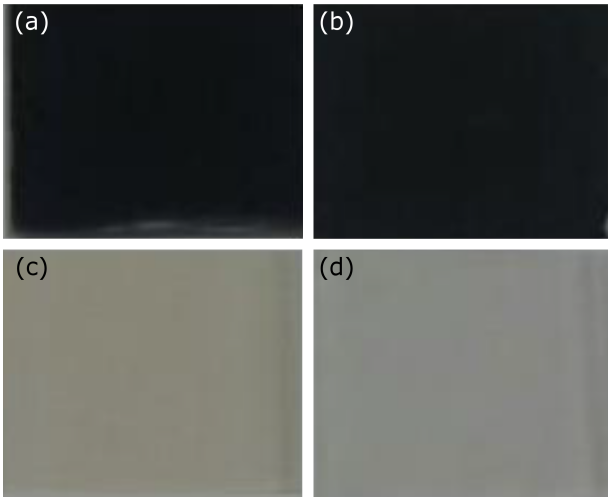

Fig. 10. Color change images of the ZnO thin films of 150 nm thicknesses with different annealing temperatures: (a) as-deposited, (b) at 200 °C, (c) at 300 °C, (d) at 400 °C.

The band gap of the ZnO films corresponding to annealing temperature for 300–400 °C was calculated by plotting $(\alpha h\nu)^2$ versus photon energy using the relation $(\alpha h\nu)^2 = \beta(h\nu - E_g)$ [21]. The energy band gap value E_g is calculated by extrapolation of the straight line of the plot are shown in Figs. 11–13. The energy band gap values changes slightly with annealing temperature. It varies from 3.41 eV to 3.31 eV for 300 °C to 400 °C for the films of 150 nm ZnO, respectively. As the film thickness increases to 250 nm, band gap values changes between 3.24 eV and 3.11 eV for 300 °C to 400 °C. For the 300 nm ZnO sample these values become 3.13 eV and 3.23 eV. As a result, optical band gap values are found in 3.11–3.41 eV range for all ZnO films.

3.4. Electrical characterization

The electrical resistivity measurements of the ZnO films obtained in this study were made using the classical van der Pauw technique. The results obtained are given in Tables II–IV. Table II gives the resistivity values of the 150 nm ZnO film set. As deposited sample with thickness of 150 nm has a sheet resistance of 34.92 Ω/□ at room temperature which contains rich Zn. After annealing (200 °C–400 °C) Zn phases shifts to the ZnO phases by entering of oxygen. This change shows itself increasingly in the sheet resistances of our film samples. Especially at 300 °C, where the transition from Zn to ZnO takes place, a sudden rise occurs in the resistance of the sample

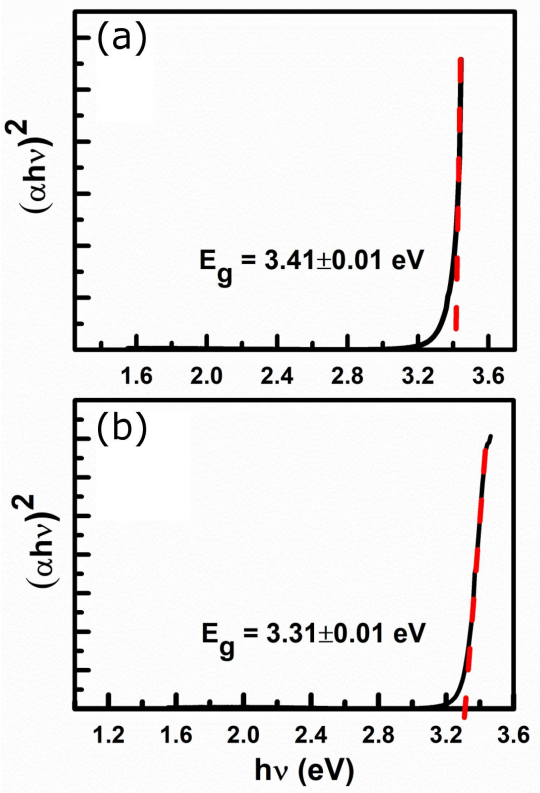

Fig. 11. The plot of $(\alpha h\nu)^2$ versus photon energy $(h\nu)$ for ZnO thin films of 150 nm annealed at various temperatures: (a) at 300 °C, (b) at 400 °C.

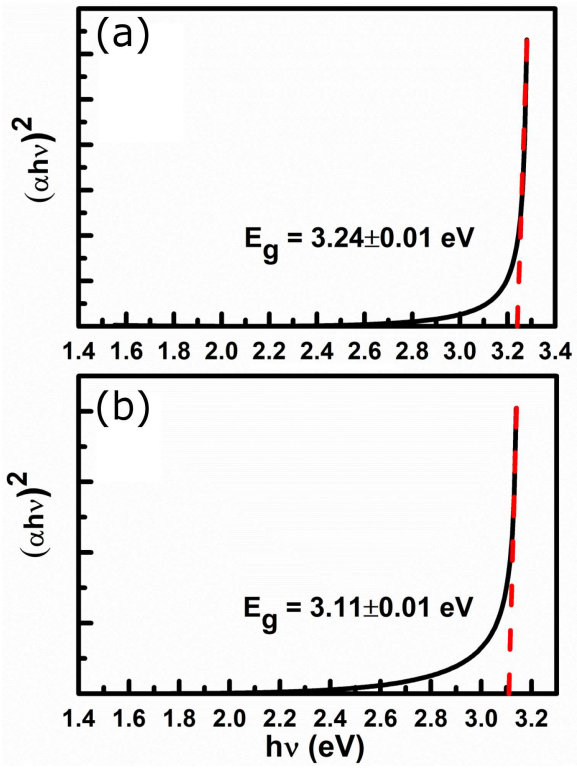

Fig. 12. As in Fig. 11, but for films of 250 nm.

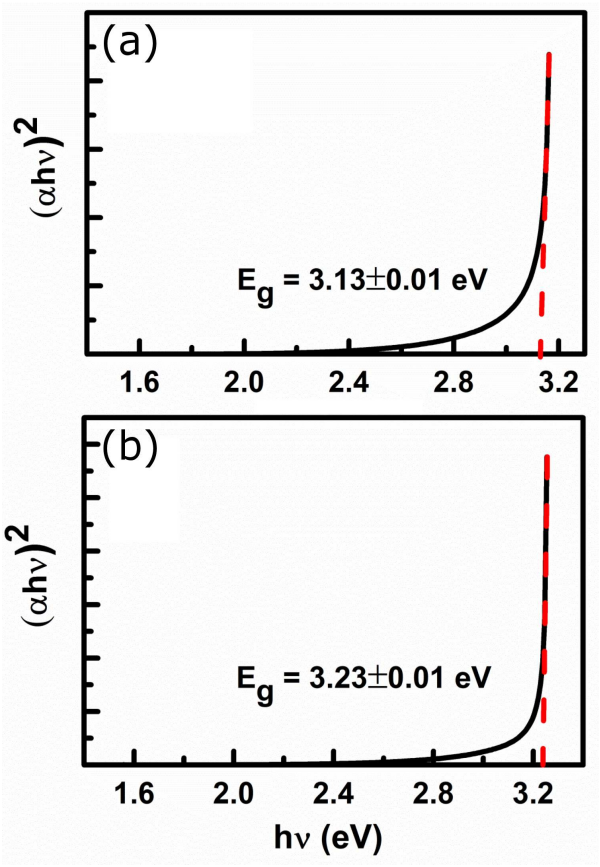

Fig. 13. As in Fig. 11, but for films of 300 nm.

TABLE II

The electrical sheet resistance and resistivity measurements (at room temp. ≈ 300 K) of the ZnO film set of 150 nm thickness

ZnO film set of 150 nm	Sheet resistance [Ω/□]	Resistivity [Ω cm]
as-deposited sample	34.92	5.2×10^{-4}
annealed at 200 °C for 2 h	941	1.4×10^{-2}
annealed at 300 °C for 2 h	3.7×10^{6}	55.5
annealed at 400 °C for 2 h	8.52×10^{6}	127.8

TABLE III

The electrical sheet resistance and resistivity measurements (at room temp. ≈ 300 K) of the ZnO film set of 250 nm thickness

ZnO film set of 250 nm	Sheet resistance [Ω/□]	Resistivity [Ω cm]
as-deposited sample	19.98	5×10^{-4}
annealed at 200 °C for 2 h	433.5	1.1×10^{-2}
annealed at 300 °C for 2 h	8.3×10^{6}	207.5
annealed at 400 °C for 2 h	14.2×10^{6}	355

TABLE IV

The electrical sheet resistance and resistivity measurements (at room temp. ≈ 300 K) of the ZnO film set of 300 nm thickness

ZnO film set of 300 nm	Sheet resistance [Ω/□]	Resistivity [Ω cm]
as-deposited sample	7.72	2.3×10^{-4}
annealed at 200 °C for 2 h	142.8	0.43×10^{-2}
annealed at 300 °C for 2 h	7.4×10^{6}	222
annealed at 400 °C for 2 h	13.6×10^{6}	408

film (3.7 MΩ/□). When we increase the annealing temperature to 400 °C, the resistance increases and the conductivity decreases slightly. These changes in electrical properties are in agreement with XRD studies. It can be explained by the fact that the peaks of the Zn phases decrease first, and then these structures completely transform to ZnO phases after annealing. Furthermore, depending on the change of the zinc-oxide phases, the light transmittance after annealing is also compatible with the change in electrical measurements. Transparency increases especially in the cases where transition from Zn-rich phase to ZnO phase is observed.

4. Conclusions

In this study, ZnO/glass film systems were obtained by thermal evaporation of highly pure ZnO particles followed by annealing in air atmosphere. The effect of annealing temperature and film thickness on ZnO formation was investigated.

XRD analyses have revealed that ZnO structures were not observed in as-deposited films. These films have only Zn phases (with low oxygen content). After annealing from 200 °C to 400 °C, these films show oxidation behavior. At 200 °C, some Zn phases reduction occurs. At 300 °C, which is important temperature in this study, Zn phases disappear and ZnO phases become visible. This indicates that the Zn phases are replaced by ZnO. In particular, (100), (002), (101), (110), (102), and (103) orientations belonging to the ZnO phases have occurred. Hence, polycrystal ZnO structures have been formed which do not have a preferential crystallographic orientation in our films obtained by thermal evaporation followed by annealing. Furthermore, XRD analyzes of our film set of 150, 250 nm, and 300 nm obtained in this study showed similar behaviors given above. Although, as the film thickness increases from 150 nm to 300 nm, intensities of the ZnO phases and crystallinity decrease.

SEM and AFM studies show that all ZnO films are formed as nanorods and completely cover the surface. In addition, clusters have formed on the surfaces of these columnar nanorods. Electrical resistivity measurements showed transition from highly conductive Zn thin film to a lower conductive ZnO films. Furthermore, optical transmittance of the ZnO films increased

to 85% after annealing. Band gap values of the ZnO films almost decreases slightly with increasing temperature and thickness. The band gap value varies between 3.11 and 3.41 eV.

Finally, we can say that from the characterization results ZnO samples with 150 nm thicknesses which were annealed at 300 °C for 2 h have the best physical properties. These ZnO nanorod structures which have good optical and electrical properties are preferred for optoelectronics and sensor applications.

Acknowledgments

This work is supported by Ege University Scientific Research Project (BAP) with Grant No. 15-FEN-058.

References

[1] N.K. Park, Y. Lee, S. Yoon, G. Han, S. Ryu, T. Lee, W. Lee, Y. Bae, *Scr. Mater.* **59**, 328 (2008).

[2] N.E. Duygulu, A.O. Kodolbas, A. Ekerim, *Phys. Status Solidi C* **11**, 1460 (2014).

[3] D. Raoufi, T. Raoufi, *Appl. Surf. Sci.* **255**, 5812 (2009).

[4] A. Zaier, A. Meftah, A.Y. Jaber, A.A. Abdelaziz, M.S. Aida, *J. King Saud Univ. Sci.* **27**, 356 (2015).

[5] P. Rai, R. Khan, R. Ahmad, Y.B. Hahn, I.H. Lee, Y.T. Yu, *Curr. Appl. Phys.* **13**, 1769 (2013).

[6] S. Singh, P. Chakrabarti, *Superlatt. Microstruct.* **64**, 283 (2013).

[7] Xue-Wen Fu, Zhi-Min Liao, Yang-Bo Zhou, Han-Chu Wu, Ya-Qing Bie, *Appl. Phys. Lett.* **100**, 223114 (2012).

[8] A. Echresh, C.O. Chey, M.Z. Shoushtari, V. Khranovskyy, O. Nur, M. Willander, *J. Alloys Compd.* **632**, 165 (2015).

[9] Yi-Fa Yang, Hua Long, Guang Yang, Aiping Chen, Qi-Guang Zheng, Pei-Xiang Lu, *Vacuum* **83**, 892 (2009).

[10] Cao Yongge, Lei Miao, S. Tanemura, M. Tanemura, Y. Kuno, Y. Hayashi, *Appl. Phys. Lett.* **88**, 251116 (2006).

[11] K. Chongsri, W. Pecharapa, *Energy Proced.* **56**, 554 (2014).

[12] R.G. Singh, F. Singh, V. Agarwal, R.M. Mehra, *J. Phys. D Appl. Phys.* **40**, 3090 (2007).

[13] Ü. Özgür, Ya.I. Alivov, C. Liu, A. Teke, M.A. Reshchikov, S. Doğan, V. Avrutin, S.J. Cho, H. Morkoç, *J. Appl. Phys.* **98**, 041301 (2005).

[14] L. Schmidt-Mende, J.L. MacManus-Driscoll, *Mater. Today* **10**, 40 (2007).

[15] Kim Kyoungwon, Yong-Won Song, Seong-Pil Chang, In-Ho Kim, Sang-Sig Kim, Sang-Yeol Lee, *Thin Solid Films* **518**, 1190 (2009).

[16] L.R. Johnson, M.Sc. Thesis, Iowa State University, 2005.

[17] R. Mariappan, V. Ponnuswamy, P. Suresh, N. Ashok, P. Jayamurugan, A.C. Bose, *Superlatt. Microstruct.* **71**, 238 (2014).

[18] A. Salman, S. Husam, M.J. Abdullah, *Measurement* **59**, 248 (2015).

[19] C.F. Wang, B. Hu, H.H. Yi, *Optik-Int. J. Light Electron Opt.* **123**, 1040 (2012).

[20] N.I. Rusli, M. Tanikawa, M.R. Mahmood, K. Yasui, A.M. Hashim, *Materials* **5**, 2817 (2012).

[21] N. Bouhssira, S. Abed, E. Tomasella, J. Cellier, A. Mosbah, M.S. Aida, M. Jacquet, *Appl. Surf. Sci.* **252**, 5594 (2006).

[22] A. Ghaderi, S.M. Elahi, S. Solaymani, M. Naseri, M. Ahmadirad, S. Bahrami, A.E. Khalili, *Pramana* **77**, 1171 (2011).

[23] S. Rajendiran, A.K. Rossall, A. Gibson, E. Wagenaars, *Surf. Coat. Technol.* **260**, 417 (2014).

[24] D. Yan, M. Hu, S. Li, J. Liang, Y. Wu, S. Ma, *Electrochim. Acta* **115**, 297 (2014).

[25] M. Mirzaee, A. Zendehnam, S. Miri, *Sci. Iran. Trans. F Nanotechnol.* **20**, 1071 (2013).

[26] K. Cai, M. Müller, J. Bossert, A. Rechtenbach, K.D. Jandt, *Appl. Surf. Sci.* **250**, 252 (2005).